Camera-based photoplethysmography in critical care patients

S. Rasche, A. Trumpp, T. Waldow, F. Gaetjen, K. Plötze, D. Wedekind, M. Schmidt, H. Malberg, K. Matschke, Sebastian Zaunseder

Angaben zur Veröffentlichung / Publication details:

Rasche, S., A. Trumpp, T. Waldow, F. Gaetjen, K. Plötze, D. Wedekind, M. Schmidt, H. Malberg, K. Matschke, and Sebastian Zaunseder. 2016. "Camera-based photoplethysmography in critical care patients." *Clinical Hemorheology and Microcirculation* 64 (1): 77–90. https://doi.org/10.3233/ch-162048.

Clinical Hemorheology and Microcirculation 64 (2016) 77–90
DOI 10.3233/CH-162048
IOS Press

Camera-based photoplethysmography in critical care patients

S. Rasche[a,*], A. Trumpp[b], T. Waldow[a], F. Gaetjen[a], K. Plötze[a], D. Wedekind[b], M. Schmidt[b], H. Malberg[b], K. Matschke[a] and S. Zaunseder[b]
[a]*Medizinische Fakultät, TU Dresden, Herzzentrum Dresden Universitätsklinik, Klinik für Herzchirurgie, Dresden, Germany*
[b]*Fakultät Elektrotechnik und Informationstechnik, TU Dresden, Institut für Biomedizinische Technik, Dresden, Germany*

Abstract.
BACKGROUND: Camera-based photoplethysmography (cbPPG) is an optical measurement technique that reveals pulsatile blood flow in cutaneous microcirculation from a distance. cbPPG has been shown to reflect pivotal haemodynamic events like cardiac ejection in healthy subjects. In addition, it provides valuable insight into intrinsic microcirculatory regulation as it yields dynamic, two-dimensional perfusion maps. In this study, we evaluate the feasibility of a clinical cbPPG application in critical care patients.
METHODS: A mobile camera set-up to record faces of patients at the bed site was constructed. Videos were made during the immediate recovery after cardiac surgery under standard critical care conditions and were processed offline. Major motion artefacts were detected using an optical flow technique and suitable facial regions were manually annotated. cbPPG signals were highpass filtered and Fourier spectra out of consecutive 10s signal segments calculated for heart rate detection. Signal-to-noise ratios (SNR) of the Fourier spectra were derived as a quality measure. Reference data of vital parameters were synchronously acquired from the bed site monitoring system.
RESULTS: Seventy patient videos of an average time of 28.6 ± 2.8 min were analysed. Heart rate (HR) was detected within $a \pm 5$ bpm range compared to reference in 83% of total recording time. Low SNR and HR detection failure were mostly, but not exclusively, attributed to non-physiological events like patient motion, interventions or sudden changes of illumination. SNR was reduced by low arterial blood pressure, whereas no impact of other perioperative or disease-related parameters was identified.
CONCLUSION: Cardiac ejection is detectable by cbPPG under pathophysiologic conditions of cardiovascular disease and perioperative medicine. cbPPG measurements can be seamlessly integrated into the clinical work flow of critical care patients.

Keywords: Camera-based Photoplethysmography, critical care patients, cutaneous microcirculation

1. Introduction

Camera-based photoplethysmography (cbPPG) is a remote method to measure pulsatile blood flow in cutaneous microcirculation. Light reflection from superficial skin layers oscillates with pulsatile changes of their blood volume, mainly due to light absorption by haemoglobin [5] and blood vessel wall movement [16]. Although subtle and invisible, these light reflections are intense enough to be sensed by cameras precisely and even over longer distances [30]. As the optical behaviour of cutaneous tissue is affected by its blood content and by pulsatile perfusion, cbPPG signals denote pivotal haemodynamic events like cardiac ejection [24].

*Corresponding author: Stefan Rasche, Medizinische Fakultät, TU Dresden, Herzzentrum Dresden Universitätsklinik, Klinik für Herzchirurgie, Dresden, Germany. E-mail: stefan.rasche@mailbox.tu-dresden.de.

The physiological principle of cbPPG is comparable to common photoplethysmographic applications like pulse oximetry in terms of signal origin, but differs substantially relating to signal detection. cbPPG signals are derived "wireless" as a two-dimensional, dynamic image, whereas conventional pulse oximetry captures only a one-dimensional tissue spot without any topical resolution.

Since the first demonstration of contactless pulse acquisition using sophisticated near infrared (NIR) cameras in 2002 [12], cbPPG with both, NIR or ambient light sources and even consumer level equipment has been proven to read heart rate and respiratory rate from a distance [29] at healthy subjects and in some clinical settings. As well, changes of oxygen saturation can be tracked by cbPPG derived parameters [27].

cbPPG has been proposed to open up convenient, contactless monitoring modalities for in- and outpatients, in occupational medicine or in preventive health care. In view of haemodynamics and microcirculation, the notable advantage of cbPPG arises from its two-dimensional imaging by a sensor matrix, compared to a single spot sensor in pulse oximetry. Thereby cbPPG is capable to visualise spatio-temporal perfusion maps, dynamic changes of cutaneous blood volume and pulse wave propagation [13, 17, 31]. Further, up to four harmonics of heart rate can be identified in Fourier transformed cbPPG signals, indicating the detection of particular features of pulse wave contour [30], [own unpublished observations]. These intrinsic characteristics of microcirculation are commonly affected in acute haemodynamic alterations like shock or sepsis [11, 23, 32]. Their assessment may be of clinical significance in critical care patients [19, 26].

However, variables with potential impact on signal strength of cbPPG, like haemoglobin concentration, body temperature or arterial blood pressure, often deviate from physiological range in those patients. As most of the current knowledge about cbPPG is derived from healthy subjects (there are only few exceptions, e.g. with dialysis patients [27] or critical ill neonates [1, 22]), the accuracy of cbPPG measurements under conditions of acute diseases remains unclear. Moreover, cbPPG measurements are sensitive to illumination, patient motion or interventions, what potentially limits their application in clinical settings. Therefore, in this paper we studied the feasibility of cbPPG measurements in critical care patients during the routine postoperative course after elective cardiac surgery, i.e. under placement of drains and tubes, routine perioperative diagnostics and procedures, and under usual lighting rather than standardised illumination.

2. Materials and methods

2.1. Patients and clinical setting

The study was approved by the Institutional Review Board of the Technical University Dresden, Germany (IRB00001473, EK168052013) and carried out at the cardiac surgical intensive care unit at the Heart Center Dresden University Hospital, Germany. Consecutive patients after elective cardiac surgery were included if they gave written, informed consent before surgery. cbPPG measurements were performed during the immediate recovery from surgery after admission at the intensive care unit.

Postoperative care followed clinical standards. Briefly, patients were kept mechanically ventilated in pressure controlled or assisted mode after transfer from the operating theatre to the ICU, until haemodynamic and respiratory conditions as well as haemostasis were stable. Cardiovascular and respiratory monitoring comprised continuous arterial and central venous pressures, a four-lead ECG, pulse oximetry, and regular blood samples. Pulmonary arterial or transpulmonal thermodilution catheters for cardiac output monitoring were placed only if indicated by cardiovascular performance during surgery or in the postoperative course. After arrival at the ICU a standard 12-lead ECG and a chest X-ray were performed and blood samples for cardiac enzymes and coagulation profile were taken.

Analgesia was provided with piritramid and metamizol. Sedatives were not given routinely. Patients were usually unconscious from continuing effects of intraoperative anaesthetics but occasionally woke up and moved slightly. Brisk awakening was treated with propofol or clonidine in individual doses. Crystalloids were infused at a rate of 150 ml/h and as boluses of 500–1000 ml in case of hypovolemia. Vasoconstrictors, vasodilators and inotropes were prescribed in line with actual recommendations [7]. External cardiac pacing by temporary atrial and ventricular wires was set at a rate of 90 bpm in DVI mode and adjusted to intrinsic cardiac rhythm and haemodynamic needs. cbPPG measurements were started, if admission procedures were completed and no immediate treatments were planned.

2.2. Technical set-up

A mobile and stand-alone measuring system with minimal impact on the clinical workflow was built (Fig. 1) [31]. The sensing system consists of two industrial CMOS cameras (IDS Imaging Development Systems GmbH), an RGB (red, green, blue) camera (UI-3370CP-C-HQ) and a near-infrared (NIR) camera (UI-3370CP-NIR-GL) with an optical NIR band-pass filter. Both cameras were equipped with lenses by Schneider Kreuznach (Cinegon 16/1.8). Spatial resolution was set to 420×320 pixels, intensity resolution (colour depth) to 12 bit ($\triangleq 4096$ steps) and temporal resolution to 100 frames per second (fps). Measurements were stored as uncompressed video data on a PC. Reference signals from the patient monitor (GE Healthcare Carescape Monitor B850) were available at sampling rates of 300 Hz or 1 Hz (300 Hz for ECG, photoplethysmogram, and continuous blood pressure, 1 Hz for trend data, e.g. systolic/diastolic blood pressure). The signals were temporarily aligned with the video recordings for later validations. A custom software was designed to start and stop the entire measurement and to store individual metadata, such as respiratory settings, pacing mode and instant medication.

The cameras were positioned at a distance between 0.6 and 1 m over the head of the patient. The video recording area captured the frontal face and upper body parts (Fig. 1). Experiments were conducted under usual ward lighting with indoor fluorescent illumination and ambient light. The luminous colour, intensity and homogeneity of the illumination varied across the measurements.

2.3. Image processing

Frontal face skin regions were selected as measurement area (region of interest – ROI), as they are easily accessible and allow a reliable vital sign extraction [18]. Standard face detection algorithms, that allow object tracking and identification of ROI movements, were not feasible in our patient setting, as they were affected by orotracheal and nasogastric tubes and their fixation tapes (Fig. 1). Furthermore, they do not trace the common variations of ambient light occurring in a clinical setting without constant, standardised illumination. Therefore, a technique to measure image velocity (also denoted as optical flow, OF) was employed, allowing both motion and light artefact detection.

Of is represented by a two-dimensional motion field within the image plane which is the projection of captured three-dimensional object velocities. Following the procedure of Barron et al. [3], we applied an OF method which adapts the image registration technique by Lucas and Kanade (Lucas-Kanade method, LKM) [21]. LKM calculates the velocity and direction for each pixel. Object movements provide motion fields of pixels with similar direction and velocities. The motion fields were processed into a one-dimensional temporary velocity signal v(t) to quantify movement. To this end, the most dominant direction of the motion field was identified and the largest region Ω, that embodies that motion at a high density (5 pixel radius), was selected. The velocity signal v(t) was derived by averaging the velocities (vector length) in Ω at the dominant direction. Our analyses showed that major changes in illumination will also be detected by LKM. Figure 2 shows an example for OF results, a detected region Ω and the velocity signal v(t).

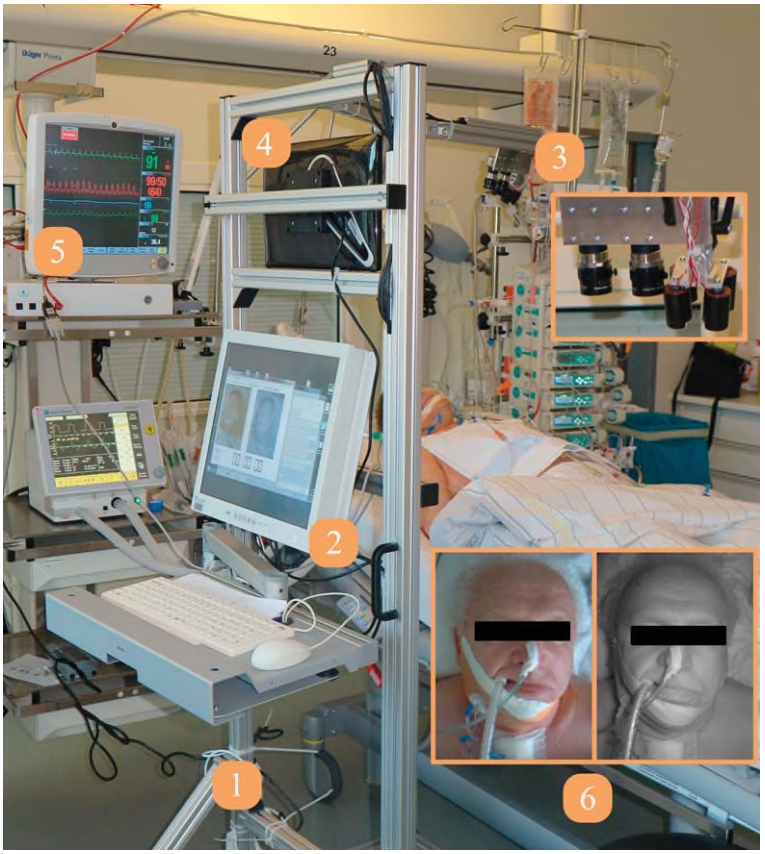

Fig. 1. cbPPG Measuring System: 1 – construction set-up, 2 – recording PC, 3 – sensing system with RGB and NIR camera (left) and NIR light source (right), 4 – additional display, 5 – GE patient monitor, 6 – video recording area (left: RGB, right: NIR).

All ROIs were selected manually. We tested that changes in v(t) appearing at $\lambda = 0.05$ pixel/s or higher (Fig. 2) might hinder separation of the cardiac signal and require a new ROI selection. For signal processing (see below), each video was divided into consecutive 10 s segments.

Segments holding velocities over λ were rated as artefact and excluded from the analyses. After any excluded segment, a new ROI was annotated using the first frame of the following 10 s-segment. For all 70 videos, a total of 404 ROI were defined. Figure 3 shows exemplary three different ROI and their use for consecutive frames.

2.4. Signal processing

In each video frame, pixel values of light reflection in the green channel within the ROI were averaged to a single intensity value. These consecutive frame values built up the photoplethysmogram with a temporary resolution of 10 ms (Fig. 3 and 4). Next, the photoplethysmogram was divided in 10 s segments for further processing. The signal segments were detrended (best straight-line fit removed) and a highpass finite impulse response (FIR) filter (cutoff frequency: 0.5 Hz, filter order: 250) was used to eliminate minor artefacts like light changes or slight movements from the signal. Fast Fourier Transform (FFT) was performed to determine the frequency spectrum of the plethysmogram. Prior Zero-Padding was employed to each segment, yielding a frequency resolution <1 bpm. Eventually, the

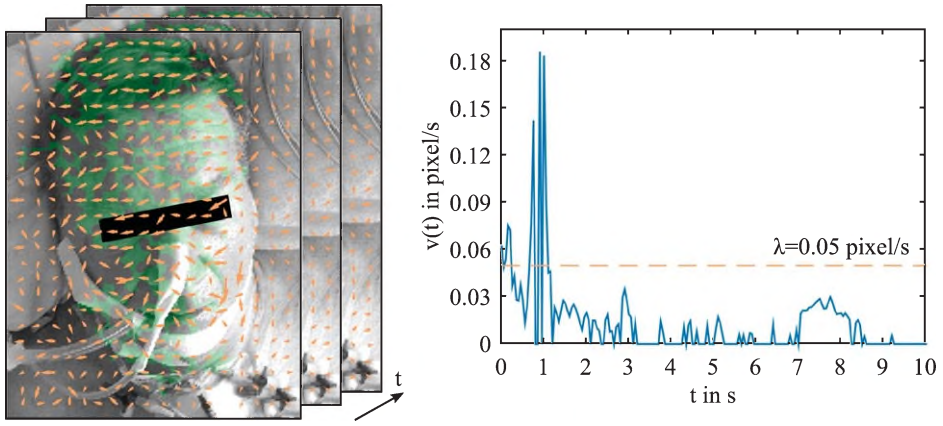

Fig. 2. Exemplary optical flow results and extracted velocity signal. Left: Frame-related motion fields (orange) - vectors at subject head similarly indicate a movement to the left side. The green region Ω marks the area of this dominant left direction. Right: Extracted velocity signal v(t) and determined threshold λ for critical movements concerning Ω.

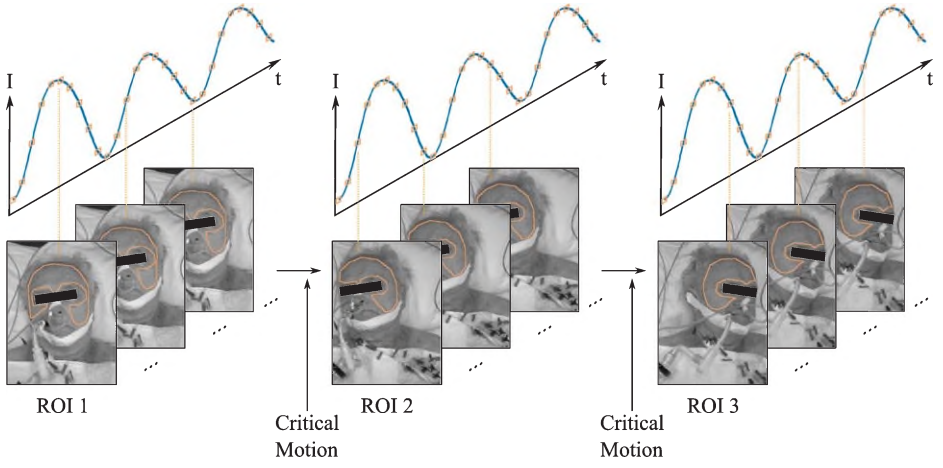

Fig. 3. Principle for ROI application and reset due to artefacts. Green pixels within the ROI are averaged to build up samples of the cbPPG signal x(t). The ROI is updated, if a head related change (movement or illumination variation) occured.

magnitudes of the FFT-segments X(f) were calculated to provide the amplitude spectra. Figure 5 shows an example for such a spectrum. Using these spectra, the maximum peak within 30 and 200 bpm was detected and its corresponding frequency considered as heart rate. Hence, the cbPPG derived heart rate (cbHR) in each 10 s segment was defined by the fundamental frequency of the colour intensity oscillations in the cbPPG signal.

To evaluate the signal quality in terms of cardiac related pulsation versus minor artefacts and technical noise degradation, a signal-to-noise ratio (SNR) was calculated, based on the formula of de Haan et al. [10]. It reads to:

$$\mathrm{SNR} = 10 \cdot \log_{10} \frac{\sum_{f=30\ bpm}^{200\ bpm} \Pi(f) \cdot |X(f)|^2}{\sum_{f=30\ bpm}^{200\ bpm} (1\text{-}\Pi(f)) \cdot |X(f)|^2} \quad (1)$$

[SNR] = dB.

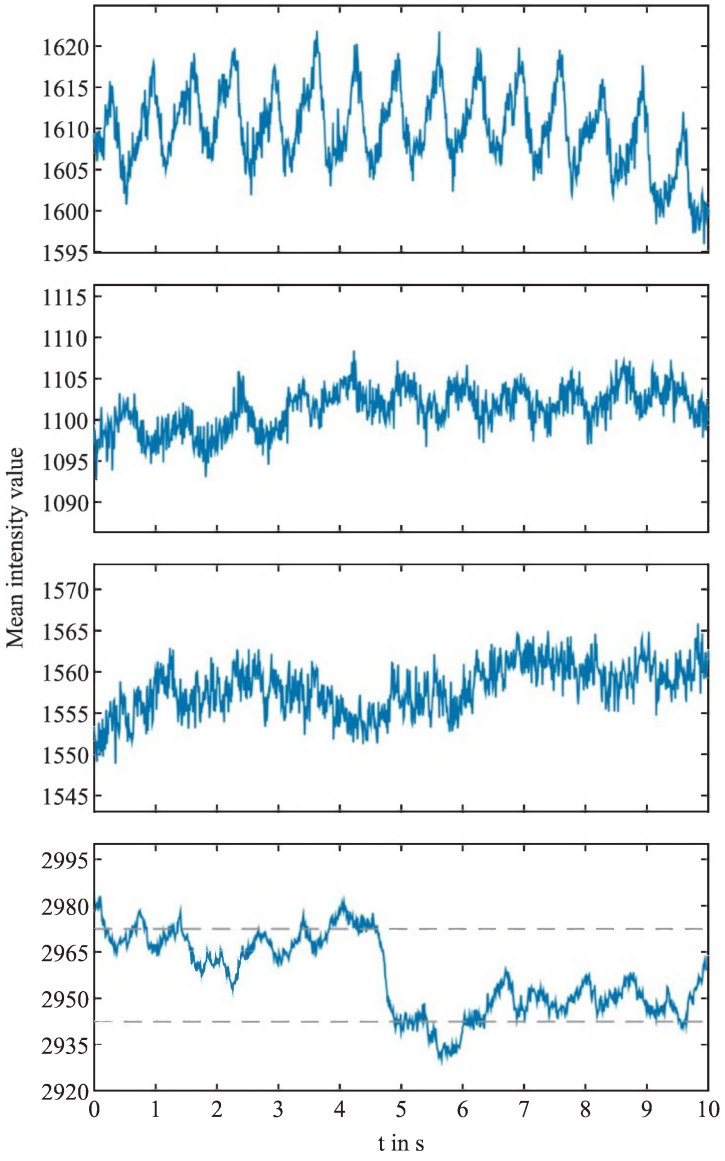

Fig. 4. Examples of unfiltered signal segments. First: Signal with high quality (no artefacts) – strong cardiac cycle related pulsation, second: Signal with moderate quality (no artefacts), third: Signal with bad quality (no artefacts), fourth: Signal with moderate quality and a minor artefact (dashed lines represent displayed area of other signals).

$|X(f)|$ describes the amplitude spectrum of a signal segment $x(t)$ and $\Pi(f)$ a masking function:

$$\Pi(f) = \begin{cases} 1 & \text{if } f \in [f_{ref} \pm 5\ bpm] \\ 1 & \text{if } f \in [2 \cdot f_{ref} \pm 5\ bpm] \\ 0 & \text{otherwise} \end{cases} \tag{2}$$

where f_{ref} depicts the segment-related reference heart rate which is derived from the monitor ECG. $\Pi(f)$ marks the signal component in the spectrum which lies at the heart rate and its first harmonic $(2 \cdot f_{ref})$. Additionally, a band of ± 5 bpm around these two frequencies is considered as well due to heart rate variabilities leading to peak blurring. Figure 5 shows these bands (orange areas) for an

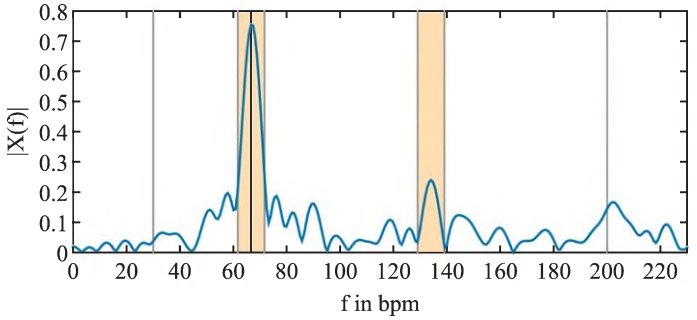

Fig. 5. Amplitude spectrum of a signal segment. The line at 70 bpm illustrates the heart frequency at the detected maximum. The lines at 30 bpm and 200 bpm represent the borders for SNR calculation: The small bands around 30 bpm and 200 bpm contain the wanted signal component, the remaining part between the outer lines the noise component.

example. The remaining values of $|X(f)|$ within 30 and 200 bpm (outer gray lines in figure 5) are considered as noise. The stronger the pulsation in $x(t)$ around the HR, and the lower the influence in other frequency ranges, the higher the SNR, and vice versa (formula 1).

2.5. Evaluation and statistics

cbPPG measurements were evaluated by cbPPG derived heart rate (cbHR) and signal-to-noise-ratio (SNR) in each 10 s video segment. Every single cbHR was compared with the average heart rate of the ECG monitoring (eHR) in the same measurement interval. Measurement error (ME) was calculated for each measurement segment as the difference between cbHR and eHR. cbHR values were rated as 'correct' or 'incorrect', if their ME was within or higher than ±5 bpm, respectively. cbPPG detection rate (DR) was calculated per patient as the number of segments with correct cbHR divided by the total number of measurement segments.

The effects of patient or treatment related factors and technical features on SNR and on the ratio of correct and incorrect cbHR readings were explored. Pseudo-replicates of multiple cbHR and SNR values per patient were precluded by averaging the variables of interest at patient level. Unadjusted bivariate comparisons were calculated by unpaired Student's *t*-test or U-test for SNR and chi-squared test for the number of cbHR readings. Differences of SNR between groups with more than two factor levels were assessed using the Kruskal-Wallis-test. Univariable and stepwise multivariable linear regression was done to identify predictors of SNR. For DR, the number of correct and incorrect cbPPG measurements was assessed by logistic regression with a generalised linear model. Finally, patients with excessive median measurement error (ME) were compared with the remaining cohort. Excessive ME were identified by $ME > Q3_{ME} + 1.5 \times IQR_{ME}$ or $ME < Q1_{ME} - 1.5 \times IQR_{ME}$ [9]. Q1 and Q3 represent the first and third quartile and IQR the interquartile range of ME, respectively. Statistics were calculated with R version 3.2.0 [25].

3. Results

160 cbPPG measurements were recorded between May and November 2014 and 70 videos further processed. Dropouts resulted from technical issues like missing reference data or loss of video images due to an unexplained drop of frame rate and sudden camera shut downs.

The study population comprised typical procedures and co-morbidities of adult patients recovering from elective cardiac surgery. Patient characteristics and details of immediate postoperative care are

Table 1
Patient and treatment characteristics

Age (years)	70.3 ± 11.4
Sex (m:w)	50:20
NYHA ≥ 2 (%)	45.8
LVEF (n)	
normal	34
mild reduced	19
moderately reduced	13
severely reduced	4
Body mass index (kg/m^2)	28.8 ± 4.1
Arterial hypertension (%)	87.1
Chronic kidney disease $\geq$ stage 2 (%)	28.6
Diabetes mellitus (%)	47.1
Coronary heart disease (%)	71.4
Peripheral arterial occlusive disease (%)	12.9
Carotid stenosis (%)	10
Surgery	
aortic valve replacement	14
coronary artery bypass graft	30
combination procedures	20
mitral valve surgery	2
other	4
Cardiopulmonary bypass time (min)	63.8 ± 33.4
Cardiac pacing	
none	20
atrial	41
ventricular or atrioventricular	9
Mean arterial blood pressure (mmHg)	77 ± 10
Heart rate (bpm)	87 ± 10
Noradrenaline infusion (%)	33
Dobutamine infusion (%)	10
Glyceryl trinitrate infusion (%)	59
Body temperature °C	36.2 ± 0.5
Haemoglobine concentration (mmol/l)	6.8 ± 0.8
Mechanical ventilation (n)	67

given in Table 1. Sixtyseven cbPPGs were recorded under mechanical ventilation and three patients were extubated in the operating theater immediately after transcatheter aortic valve implantation.

A total of 12672 segments were explored. 12021 segments (94.9%) were further processed and 651 discarded because of movement and illumination artefactes detected by OF. The mean duration of cbPPG analysis per patient was 28.6 ± 2.8 min.

cbHR, i.e. the rate of pulsatile cutaneous perfusion detected by cbPPG, matched the heart rate in the ECG reference monitoring (eHR $\pm$ 5 bpm) in 9974 of 12021 segments, or 83% of total recording time. The median detection of heart rate per patient was 92.6% (IQR 78.9–98.9%). cbHR had an overall bias (mean difference to eHR) of -3.7 ± 16.1 bpm. Measurement errors (ME) were predominantly negative (87.3%) and 69.9% of them differed from their reverence value between –20 and –50 %. (Fig. 6). Correct cbPPG measurement showed a mean cbHR bias of -0.1 ± 0.8 bpm. Signal-to-noise ratio (SNR) ranged between –29.4 and +10.9 (median 0.89, IQR –3.56; 4.40). ME decreased clearly

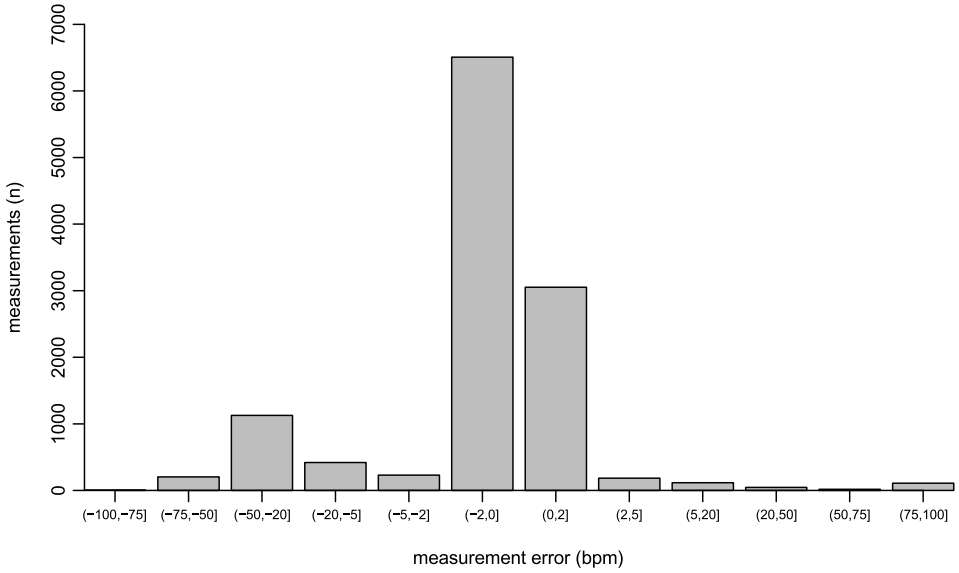

Fig. 6. Distribution of measurement errors.

at higher SNR values (Fig. 7a). The detection rate of pulsatile perfusion (DR) approximates 100% at the highest SNR values (Fig. 7b).

3.1. Influence of perioperative and critical care conditions

Univariable regression showed a small but significant rise of SNR and DR with increasing mean arterial blood pressure. Higher image intensity caused an increase of SNR, but not of DR. Conversely, DR was higher at patients with dobutamine infusion, whereas SNR was not. The effects of blood pressure remained significant in stepwise multivariable analysis, but showed only a small r^2 (Table 2). Other patient characteristics or perioperative conditions had no obvious influence on DR or SNR.

cbPPG performance appeared to vary between surgical procedures and ventilation patterns, as suggested by differences in SNR and DR (Table 3). Highest values were measured in patients with aortic valve replacement, followed by CABG surgery and combination procedures at least. Likewise, the three patients not mechanically ventilated showed higher SNR and DR. However, all of these differences were not statistically significant.

Patients with excessive median measurement error differed from the remaining cohort only in terms of SNR and a lower mean arterial blood pressure. However, albeit statistically significant, the difference in mean arterial blood pressure was small and only of minor clinical relevance (72 ± 8 mmHg vs. 78 ± 10 mmHg, $p = 0.037$, Table 4).

4. Discussion

The concept of remote, camera-based photoplethysmography has been introduced several years ago [12] and was investigated in numerous studies, mainly with healthy volunteers. In this study, we applied the method in critical care patients with profound cardiovascular diseases requiring surgical treatment, and under the immediate conditions after major surgery and anaesthesia.

We analysed time-varying intensity changes of reflected light in the green channel. It has been shown previously that reflection of green light provides the strongest photoplethysmographic signal

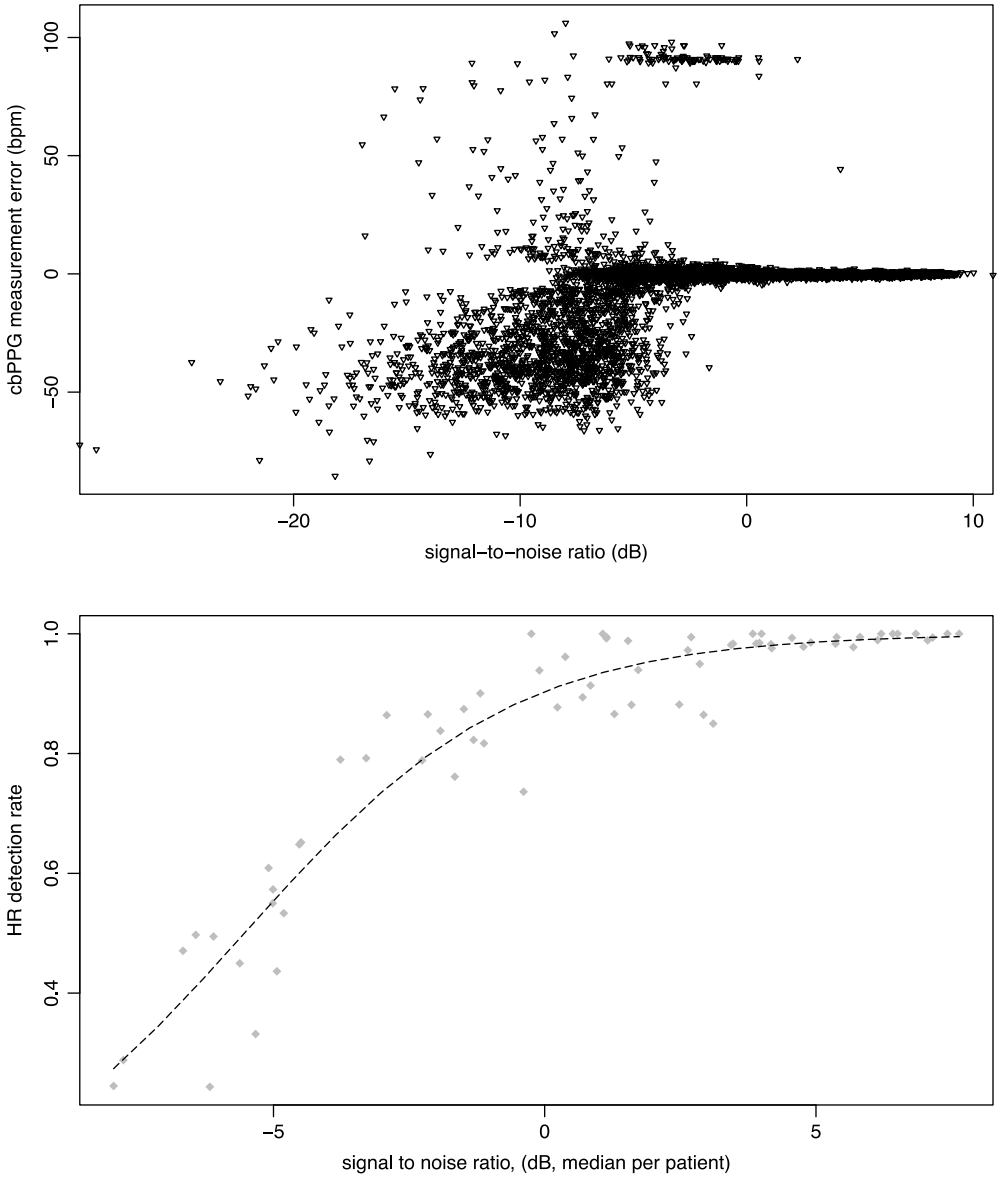

Fig. 7. measurement error of all segments (top) and correct detection of heart rate per patient (bottom) in relation to SNR.

because of spectral absorption maxima of oxygenated and deoxygenated haemoglobin [30], as well as a result of sensor architecture. Considering a penetration depth of green light of about 1mm [4], and a non-pulsatile blood flow in capillaries, the pulsatile plethysmographic signal in our setting is likely to arise from smallest blood vessels described as the upper horizontal arteriolar network in the papillary dermis [6, 14].

Light absorption of haemoglobin is suggested as the pivotal link between time-varying optical properties and pulsatile blood volume in the tissue, but alternative mechanisms like blood vessel wall movement and deformation of connective tissue by arteriolar transmural pressure have been proposed [15]. Together, these mechanisms provide a signal oscillation proportional to changes in cutaneous blood volume associated with cardiac ejection. This feature and its two-dimensional sensoring matrix render the clinical significance of cbPPG measurements beyond solely estimating heart rate. cbPPG

Table 2

Linear regression of Signal to noise ratio (SNR) and logistic regression of pulse detection rate using a generalised linear model with quasibinomial error structure. For multivariable regression, non-significant interaction terms were deleted stepwise. For SNR, model $r^2 = 0.283$, model probability $p = 0.006$. For DR, model r^2 (McFadden) = 0.237, model probability < 0.001. ABP, arterial blood pressure; CBP, cardiopulmonary bypass; LVEF, left ventricular ejection fraction

	SNR				Pulse detection rate		
Univariable	ß	95% CI	*p*		OR	95% CI	*p(q)*
Image intensity	**0.151**	**0.054 – 0.248**	**0.003**		1.027	0.990 – 1.066	0.168
Movement	0.496	–1.288 – 2.280	0.581		1.119	0.605 – 2.106	0.722
Mean ABP	**0.112**	**0.009 – 0.215**	**0.034**		**1.053**	**1.013 – 1.099**	**0.001**
Temperature	–0.526	–2.624 – 1.572	0.619		0.815	0.403 – 1.677	0.574
Haemoglobine	–0.796	–2.127 – 0.536	0.237		1.025	0.646 – 1.636	0.918
CBP time	0.019	–0.014 – 0.049	0.264		1.010	0.999 – 1.022	0.081
Body mass index	–0.057	–0.316 – 0.203	0.665		0.969	0.889 – 1.060	0.485
Age	0.013	–0.080 – 0.106	0.784		1.008	0.975 – 1.036	0.628
Cardiac pacing							
none	reference				reference		
atrial	–1.533	–3.887 – 0.821	0.198		0.562	0.209 – 1.345	0.223
ventricular	–3.368	–6.832 – 0.096	0.565		0.396	0.119 – 1.319	0.130
LVEF							
normal	reference				reference		
mild	–0.490	–3.029 – 2.049	0.701		1.316	0.561 – 3.319	0.542
mod	0.169	–2.722 – 3.060	0.907		0.644	0.381 – 2.538	0.904
severe	2.298	–2.388 – 6.984	0.331		3.245	0.529 – 90.732	0.315
Noradrenaline	–0.737	–2.974 – 1.499	0.513		1.011	0.475 – 2.260	0.977
Dobutamine	1.965	–1.515 – 5.445	0.264		**16.875**	**1.724 – 14705**	**0.009**
Glyceryl trinitrate	–0.543	–2.678 – 1.592	0.613		0.835	0.387 – 1.745	0.637
multivariable	ß	95% CI	*p*		OR	95CI	*p(q)*
Image intensity	**0.145**	**0.005 – 0.240**	**0.003**	**dobutamine**	**18.236**	**2.040 – 8346**	**0.083**
Mean ABP	**0.102**	**0.004 – 0.199**	**0.041**	**mean ABP**	**1.054**	**1.020 – 1.100**	**0.007**

yields dynamic perfusion maps allowing the evaluation of spatio-temporal blood volume distribution and pulse wave propagation [17, 31]. These distinct informations about the cutaneous circulation are not yet well established in the care of critically ill patiens. However, perfusion assessment of non-vital organs like the skin is suggested to be incorporated into therapeutic strategies [19], as it has been proven predictive of worsening organ function in septic shock [2, 20] and of a complicated course after major abdominal surgery [28]. Of note, the quantitative relation of the cbPPG signal and the cutaneous blood flow rather than the cutaneous blood volume remains to be investigated.

We validated cbPPG comparing its fundamental frequency with the heart rate taken from the ECG reference monitoring. Eighty-three percent of all cbPPG measurements (83% of cbPPG analysis time) were considered correct and showed a close agreement between cbPPG derived heart rate and its reference (mean difference -0.1 ± 0.8 bpm). This fact as well as the increasing detection rate and the nearly vanishing measurement error with higher signal quality indicate that cbPPG may detect pulsatile cutaneous blood volume changes precisely under critical care conditions. Other studies with cbPPG in different settings showed comparable results. cbPPG yielded heart rate with a mean measurement error of 2.52 bpm in neonates [22] and of approximately 3 bpm in dialysis patients [27]. Compared to the 17% of analysis time with failing cbPPG measurements and the predominant measurement

Table 3
Signal to noise ratio and detection rate in different surgical procedures and ventilation patterns. AVR, aortic valve replacement; CABG coronary artery bypass graft

Surgery	SNR	DR
AVR	2.67 ± 4.04	89.9 ± 17.0
CABG	0.74 ± 4.29	84.1 ± 20.9
Combination procedures	-0.81 ± 4.35	78.3 ± 23.0
Mitral valve surgery	0.96 ± 4.55	88.2 ± 12.2
Other	0.47 ± 5.76	79.3 ± 33.8
	$p = 0.2538$	$p = 0.5847$
Ventilation		
Mech. ventilated	1.07 ± 4.43	91.4 ± 21.6
Spont. breathing	3.90 ± 1.22	98.4 ± 5.93
	$p = 0.24$	$p = 0.504$

Table 4
Comparison between patients with excessive measurement errors (outliers) and the remaining group

	group	outliers	p
Detection rate (%)	97.7 (86.6 – 99.3)	48.5 (24.3 – 60.9)	
Image intensity	33.2 ± 10.1	28.3 ± 10.5	0.159
Movement	0.01553 ± 0.00613	0.01532 ± 0.00510	0.898
Signal to noise ratio (dB)	2.55 (–0.35 – 4.72)	–5.86 (–6.49 – –5.01)	<0.001
Mean arterial blood pressure (mmHg)	78.0 ± 10.2	72.3 ± 7.6	0.037
Body temperature (°C)	36.2 ± 0.45	36.3 ± 0.72	0.981
Haemoglobine concentration (mmol/l)	6.8 ± 0.8	6.8 ± 0.9	0.973
Cardiopulmonary bypass time (min)	65.7 ± 34.1	54.4 ± 29.6	0.149
Body mass index (kg/m^2)	28.9 ± 4.1	28.3 ± 4.1	0.668
Age (years)	70.2 ± 12.0	70.6 ± 8.6	0.79
Cardiac pacing			0.078
none	18	2	
atrial	35	6	
ventricular	5	4	
LVEF			0.657
normal	27	7	
mild reduced	17	2	
moderately reduced	10	3	
severely reduced	4	0	
Norepinephrine (n) no / yes	39 / 19	8 / 4	1
Dobutamine (n) no / yes	51 / 7	12 / 0	0.343
Glyceryl trinitrate (n) no / yes	23 / 35	6 / 6	0.734

error between –20 to –50 bpm in our study, a cbPPG setting in adults [8] showed a 20% error rate in identifying patient's heart rhythm as atrial fibrillation or not, and left 5% to 17% of heart beats undetected.

Measurements were barely affected by haemodynamic or treatment related variables. Especially, preoperative left ventrcular ejection fraction, cardiac pacing, haemoglobin concentration, body

temperature or therapy with norepinephrine or glyceryl trinitrate did not influence the cbPPG specifications. Higher mean arterial blood pressure, treatment with dobutamine and image intensity slightly enhanced signal acquisition. These effects were small and explained a merely little proportion of the observed variability ($r^2 = 0.28$ for SNR and $r^2 = 0.24$ for DR). Increasing cbPPG signal strength and detection of cardiac pulse in superficial skin layers with heigher blood pressure or dobutamine infusion might hint at an increased cutaneous perfusion. It has to be noted, that this issue was neither assessed quantitatively nor in its two-dimensional characteristics in this study. Further investigations are needed to elucidate the very capability of cbPPG to examine these microcirculatory features in various clinical situations. Signal analysis in the red and near infrared channel might reveal more detailed information about perfusion in deeper skin layers, including the lower plexus and postcapillary venules. Additionally, advancements of signal processing aiming to describe the strength and spatio-temporal distribution of the cbPPG signal is in the scope of further studies.

The 17% measurement failures in our study could not be clearly attributed to patient or treatment related variables. Also the large range of detection rates of cardiac pulse between patients, from 24.3% to 100% (median 92.6%), had no obvious pathophysiological or treatment related reason, as those 13 patients with an excessive median ME and a correspondingly low detection rate did not show major differences to the remaining cohort. Importantly, functional arteriovenous anastomoses in lower cutaneous blood vessels may cause blood flow to bypass superficial layers in response to autonomous and thermal regulation [5], presumably in pathophysiological situations like recent surgery, anaesthesia and extracorporal circulation. Again, these microcirculatory variations are not necessarily reflected by macrohaemodynamic variables and therefore may be left undetected in our analyses. Other circumstances, which could contribute to cbPPG measurement failures include individual variations of dermal and epidermal thickness with consecutive physical limitations of penetration depth, different pigmentation patterns and dissimilarities in microvascular anatomy of the papillary dermis.

5. Conclusion

Results of this study prove the feasibility of cbPPG in a perioperative, critical care patient cohort. cbPPG measurements reflect pulsating cutaneous blood flow precisely and common aspects of critical care did not impede cbPPG measurements substantially. Further studies are required to quantify cutaneous blood volume pulse and to describe its spatio-temporal characteristics by cbPPG.

References

[1] L.A.M. Aarts, et al., Non-contact heart rate monitoring utilizing camera photoplethysmography in the neonatal intensive care unit — A pilot study, *Early Human Development* **89**(12) (2013), 943–948.

[2] H. Ait-Oufella, et al., Capillary refill time exploration during septic shock, *Intensive Care Medicine* **40**(7) (2014), 958–964.

[3] J.L. Barron et al., *Performance of Optical Flow Techniques*, London : Department of Computer Science, University of Western Ontario, (1993).

[4] A.N. Bashkatov, et al., Optical properties of human skin, subcutaneous and mucous tissues in the wavelength range from 400 to 2000 nm, *Journal of Physics D: Applied Physics* **38**(15) (2005), 2543–2555.

[5] E. Berardesca, et al., EEMCO Guidance for the Measurement of Skin Microcirculation, *Skin Pharmacology and Physiology* **15**(6) (2002), 442–456.

[6] I.M. Braverman, The cutaneous microcirculation: Ultrastructure and microanatomical organization, *Microcirculation (New York, N.Y. : 1994)* **4**(3) (1997), 329–340.

[7] M. Carl, et al., S3 Guidelines for intensive care of cardiac surgery patients, *Zeitschrift für Herz-,Thorax- und Gefäßchirurgie* **24**(5) (2010), 294–310.

[8] J.-P. Couderc, et al., Detection of atrial fibrillation using contactless facial video monitoring, *Heart Rhythm* **12**(1) (2015), 1–7.
[9] M.J. Crawley, Statistik mit R. John Wiley & Sons 2012.
[10] G. de Haan and V. Jeanne, Robust Pulse Rate From Chrominance-Based rPPG, *IEEE Transactions on Biomedical Engineering* **60**(10) (2013), 2878–2886.
[11] C.G. Ellis, et al., The microcirculation as a functional system, *Critical Care* **9** (Suppl 4) (2005), S3–S8.
[12] M. Huelsbusch and V. Blazek, Contactless mapping of rhythmical phenomena in tissue perfusion using PPGI, *SPIE* **4683**, (2002), 110–117.
[13] R. Imms, et al., A high performance biometric signal and image processing method to reveal blood perfusion towards 3D oxygen saturation mapping, (2014), 89470X–11.
[14] F. Jung, et al., Laser Doppler flux measurement for the assessment of cutaneous microcirculation – critical remarks, *Clinical hemorheology and microcirculation* **55**(4) (2013), 411–416.
[15] A.A. Kamshilin, et al., A new look at the essence of the imaging photoplethysmography, *Nature Publishing Group* (2015), 1–9.
[16] A.A. Kamshilin, et al., Photoplethysmographic imaging of high spatial resolution, *Biomedical optics express* **2**(4) (2011), 996–1006.
[17] A.A. Kamshilin, et al., Variability of Microcirculation Detected by Blood Pulsation Imaging, *PLoS ONE* **8**(2) (2013), e57117–9.
[18] G. Lempe, et al., ROI Selection for Remote Photoplethysmography. Bildverarbeitung für die Medizin 2013, *Springer Berlin Heidelberg* (2013), 99–103.
[19] A. Lima and J. Takala, Clinical significance of monitoring perfusion in non-vital organs, *Intensive Care Medicine* **40**(7) (2014) 1052–1054.
[20] A. Lima, et al., The prognostic value of the subjective assessment of peripheral perfusion in critically ill patients, *Critical Care Medicine* **37**(3) (2009), 934–938.
[21] B.D. Lucas and T. Kanade, An iterative image registration technique with an application to stereo vision, *IJCAI* (1981).
[22] L.K. Mestha, et al., Towards continuous monitoring of pulse rate in neonatal intensive care unit with a webcam, (2014), 3817–3820.
[23] J. Nantais, et al., Impact of methylene blue in addition to norepinephrine on the intestinal microcirculation in experimental septic shock, *Clinical hemorheology and microcirculation* **58**(1) (2014), 97–105.
[24] A. Reisner, et al., Utility of the Photoplethysmogram in Circulatory Monitoring, *Anesthesiology* **108**(5) (2008), 950–958.
[25] J. Ruffell, et al., Discriminating the Drivers of Edge Effects on Nest Predation: Forest Edges Reduce Capture Rates of Ship Rats (Rattus rattus), a Globally Invasive Nest Predator, by Altering Vegetation Structure, *PLoS ONE* **9**(1) (2014), e113098.
[26] N. Sharawy and C. Lehmann, New directions for sepsis and septic shock research, *The Journal of surgical research* **194**(2) (2015), 520–527.
[27] L. Tarassenko, et al., Non-contact video-based vital sign monitoring using ambient light and auto-regressive models, *Physiological Measurement* **35**(5) (2014), 807–831.
[28] M.E. van Genderen, et al., Clinical assessment of peripheral perfusion to predict postoperative complications after major abdominal surgery early: A prospective observational study in adults, **18**(3) (2014), 1–13.
[29] W. Verkruijsse and M.P. Bodlaender, A novel biometric signature: Multi-site, remote (>100m) photo-plethysmography using ambient light, (2010).
[30] W. Verkruysse, et al., Remote plethysmographic imaging using ambient light, *Optics express* **16**(26) (2008), 21434–21445.
[31] S. Zaunseder, et al., Multivariate biosignal acquisition to assess the potential of remote photoplethysmography, *Biomedical Engineering/Biomedizinische Technik* **57** (2012), SI–1. Track-O (2012), 1–1.
[32] J. Zhou, et al., Physostigmine reverses disturbances of the intestinal microcirculation during experimental endotoxemia, *Clinical hemorheology and microcirculation* **56**(3) (2014), 273–284.